Analysis and Simulation of Three-Input DC-DC Converter with Bipolar Symmetric Outputs

Narjis Muayad Majeed* and *Turki Kahawish* Hassan

Department of Electrical Engineering, Mustansiriyah University, Baghdad, Iraq

Abstract .This paper presents a three-input high-gain DC-DC converter with bipolar symmetric outputs. The advantages of a bipolar DC grid are higher reliability, flexibility, and efficiency as compared with the unipolar DC grid. Therefore, the proposed converter is designed to connect directly with the bipolar DC grid due to its bipolar symmetric outputs. The three input voltage sources to the converter are operated in a sequential manner from the first voltage source to the last one, with each source providing power at a level proportional to its duty cycle. Similarly, when the sources are equal, they operate in a sequential manner with their specific power. In addition, the proposed converter is designed to provide the required power to the grid under both simultaneous or individual from three input voltage sources. A double-loop PI controller is applied to regulate the converter output voltages and the control loop is analyzed and the transfer function relating reference voltage to output voltage is derived. Voltage balance control is provided to ensure that the outputs remain symmetrical despite changes in load conditions or input voltage. A converter with a power rating of 1000W and output voltage levels of 200V, -200V, and 400V is designed. The three supply voltage of 150V,100V, and 75V are used. The converter is tested under a variation of supply voltages and load using MATLAB/SIMULINK. The results show the feasibility and effectiveness of the proposed converter.

1 Introduction

All-electric hybrid energy sources are becoming very important [1] and zero-emission forms of transportation, such as electric vehicles and ferry boats [2]. The combination of electric energy systems needs the simultaneous operation of a number of electric energy sources, and systems having energy storage components must maintain bidirectional operations at all times. Topologies of multiple-input DC-DC power converters are commonly used for integrating energy sources [3], [4]. These energy sources include wind turbines, fuel cells, solar panels, and ultra-capacitors. They allow power to flow from different voltage sources to the output [5], [6]. Wind and photovoltaic (PV) energies have a complementary relationship as periods of sunshine are frequently accompanied by low wind conditions, while periods of cloud cover throughout either day or night tend to generate strong winds. The integration of PV modules and wind energy modules results in a reduction in periods of electricity unavailability. Hybrid solar, fuel cell and wind generators have been found to offer a higher level of consistency and reliability in electricity provision compared to alternative singular sources, [3]. Multi-source conversions utilizing conventional single-input converters would necessitate the construction of a complex and expensive structure, leading to a substantial increase in expense [7], [8]. An integrated multi-input DC-DC converter can be used instead of connecting several DC-DC converters to different sources separately. These converters have a low number of components, less space, cost less, and have better dynamic performance [9-15]. According to whether they are connected to the grid or not, microgrids can be categorized as DC microgrids or AC microgrids. The DC microgrid is common in a lot of our lives, including photovoltaic (PV) generation, energy storage systems, light emitting diode(LED), and electric vehicles [16]. DC microgrid construct can be divided into two main categories: (i) Unipolar and (ii) Bipolar. The bipolar DC microgrid (BDCMG) architecture has more choices for loads and distributed generation because it has two voltage levels. It also has a high level of efficiency and quality [17], [18]. Further, the reliability of BDCMG is high because even if one wire fails, the other two connections can still send power to the load [19], [20]. Because of these benefits, BDCMG is the best choice for applications that need to be highly efficient and reliable. A central voltage balancer is needed in a bipolar DC microgrid to keep the voltages at the upper and lower terminals equal, even when the loads aren't balanced [21]. It is very important for a bipolar DC microgrid to have a symmetrical bipolar output voltage in order to work in places like an electric car charging station and a data center power supply system. The unbalanced volts are not good because they lower the quality of the power, put more stress on semiconductor devices, and, in the worst case, damage the whole power conversion system [16], [22], [23].

* Corresponding author: narjis.m.majeed@uomustansiriyah.edu.iq

Converters with several dc-dc inputs may be non-isolated or isolated. There has been a proposal in [24–25] that isolated multi-input converters (MICs) are designed for operation in circuits that are coupled inductors or transformers, which create magnetic coupling. On the other hand, it was suggested in [19–23,26,27] that non-isolated MICs work with circuits that are electrically connected. A proposal for MPC with multiple inputs and outputs (MIMO) is suggested in reference [28]. Nevertheless, the output ports of this MIMO must deal with voltage cross-regulation, which requires the implementation of complicated controllers to reduce this problem. The non-isolated counterparts in [27, 29], the bipolar DC circuit cannot receive power independently from either of the input sources. Additionally, they require a lot of complicated control to maintain symmetrical and balanced output voltages. The non-isolated MPC suggested in [30] employs two sources of input using different and equal voltage levels. However, power cannot be sent to the load simultaneously without following specific regulations. At different voltages, levels of the sources are arranged in descending order: $V_1 > V_2 > \cdots > V_N$, PWM signals should have duty cycles of $D_1 < D_2 < \cdots < D_N$, and when the voltages are equal, the other sources produce more time of operation compared to the first source. In order to resolve the aforementioned problems, this study introduces a non-isolated three-input DC-DC converter which includes bipolar symmetric outputs. The proposed converter offers notable properties:

1) The suggested converter will be analyzed with three different input sources that have different and similar voltage levels. In all cases, the input voltage will be operated sequentially with the duty cycle assigned to each input.
2) Power flow can occur simultaneously or independently from three different sources to the bipolar DC link.
3) Voltage balancing control is employed to keep the symmetry of the outputs in the presence of fluctuating load situations or variations in input voltage.
4) The duty cycles of the PWM signals used to control the input sources of power are regulated by a basic controller, like the conventional double-loop PI controller, which employs an Exclusive OR Gate between the duty cycles that have been produced to guarantee sequential and non-overlapped operation.
5) By utilizing switched inductor cells, the voltage gain of the proposed converter is high.
6) Continuous conduction mode (CCM)is assumed for the operation of the proposed converter.

The following sections summarize the parts of this paper: Section 2 discusses steady state analysis, independent power flow, and voltage and current stress of transistors and diodes. Section 3 illustrates the control structure and DC Voltage Balancing Control. Section 4 contains simulation results and discussions. Finally, the conclusion in Section 5.

2 Proposed Converter

Three-input DC-DC converters with bipolar symmetric outputs are depicted in Fig.1. The topology consists of three input power sources, namely V_1, V_2, and V_3. The circuit consists of 6 control switches (Switch S_1, S_2, S_3, S_4, S_p, and S_n), five diodes, three inductors, two capacitors, and three DC loads with different values connected to the positive and negative poles. R_1 and R_2 indicate the corresponding loads of the bipolar bus and R_t for the output load. Additionally, the converters can provide three voltage levels on the DC connections, namely $\pm V_o/2$ and V_o.

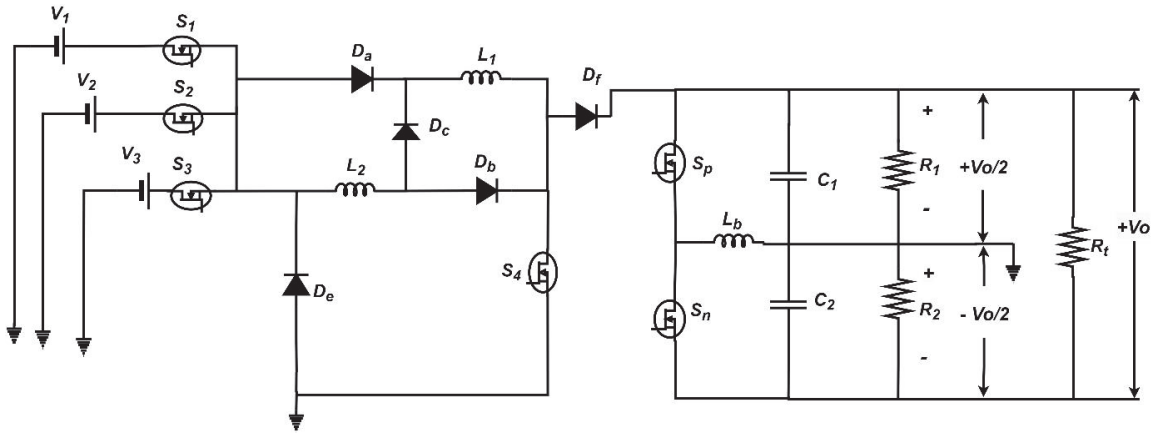

Fig. 1. Proposed converter circuit.

2.1 Steady State Analysis of the Proposed Converter

Fig.2 shows the flow of current during charging and discharging of inductors at steady-state operation. As shown in Fig. 3 during the first part of the period Ts, which is ($\sum_{i=1}^{3} D_i T_S$), the three switches (S_1–S_3) are ON in a sequential manner with duty cycles of D_1, D_2, and D_3 respectively, and S_4 is turned ON in the whole of this part of the period, and the inductors

(L_1 and L_2) are charged. During the second part of the period, which is $(1 - \sum_{i=1}^{3} D_i)T_S$, all the active switches (S_1–S_4) are OFF, and the inductors (L_1 and L_2) are discharged. The charging of each inductor has a slope of$(\sum_{i=1}^{3} D_i V_i)/L)$. This charging occurs when diodes D_a and D_b are in a forward-biased state, while D_e, D_f, and D_c are reversed-biased. All inductors discharge with a slope of $(-V_o/4)/L$ with diodes D_e, D_f, and D_c are forward-biased, while D_a and D_b are reverse-biased. As shown in Fig. 2 the bipolar dc bus switches S_P and S_n are sequentially operated with duty cycles of 50% to ensure that the bipolar output voltages are balanced.

When the inductance voltage-second balancing concept is applied to the steady-state inductor voltage waveform shown in Fig. 3, the output voltage, which is denoted by (1), may be described as follows:

$$V_o = 4[(\sum_{i=1}^{3} V_i D_i)/(1 - \sum_{i=1}^{3} D_i) \qquad (1)$$

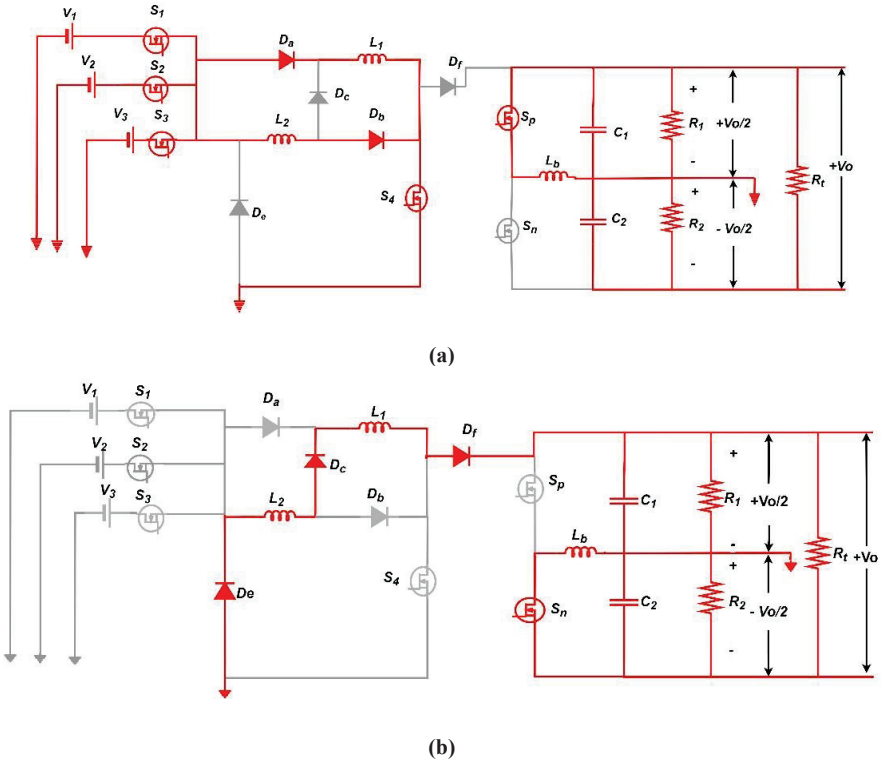

(a)

(b)

Fig.2. The flow of current during the (a) charging and (b) discharging of an inductor in a condition of a steady state operation.

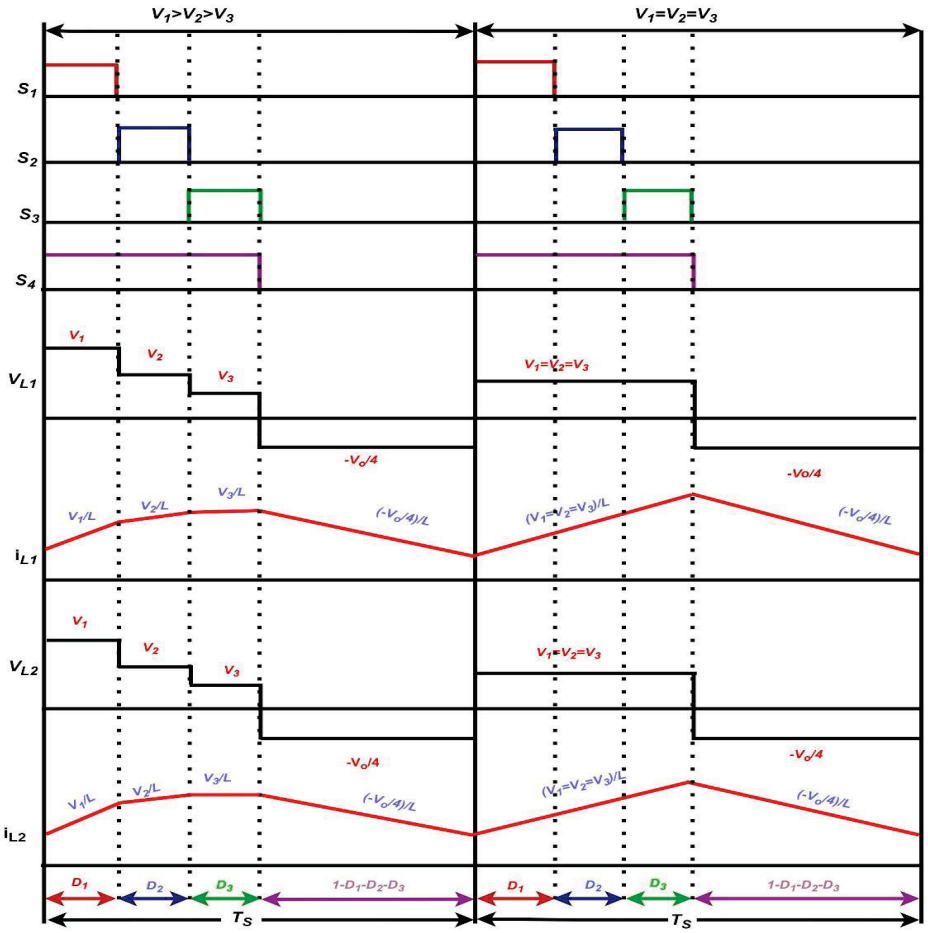

Fig. 3. CCM steady-state waveform

Fig.3 shows the source voltage magnitudes with ($V_1 > V_2 > V_3$) for unequal voltage. The first voltage source (V_1) continues to work until the end of D_1T_S. After that, the second source will continue to operate until the end of D_2T_S. Lastly, the third source will continue to operate until the end of D_3T_S. Similarly, when the source voltages are equivalent, as shown in $V_1 = V_2 = V_3$. The duty cycle D_4 applied to S_4 is equal to the sum of the duty cycles of the switches controlling the input ports (S_1, S_2, and S_3).

2.2 Independent Power Flow

The converter operates in the independent power flow mode, this is one of the important features of the proposed converter, which is its ability to transfer power to the bipolar dc bus from any of the inputs, (V_1, V_2, or V_3) for a three-input converter. Each input source is controlled by its own switch, S_1 for V_1, S_2 for V_2, and S_3 for V_3. It starts with V_1 being on to charge the inductors. For D_1T_S, S_1 and S_4 are both on with the same duty cycle (D_1), but S_2 and S_3 are off during the switching period. In the same way, when V_2 is needed to provide power to the dc link, S_2, and S_4 are both active at the same duty cycle (D_2), while S_1 and S_3 remain OFF throughout the switching period if V_3 supply the dc link, for inductor charging, S_3, and S_4 are switched ON with the same duty cycle (D_3) while S_1 and S_2 are off.

2.3 Voltage and Current Stress

When choosing power switches and diodes, it is essential to consider the voltage stress and current stress. The voltage stress is defined as the maximum voltage magnitude across a power electronic switch during its off state.

The voltage stress of S_1, S_2, S_3, and S_4 shown below.

$$V_{S1} = V_{S2} = V_{S3} = \text{Max}(V_1, V_2, V_3) \quad (1)$$

$$V_{S4} = \frac{V_o}{2} \quad (2)$$

The voltage stress of S_p and S_n are provided below.

$$V_{Sp} = V_{Sn} = V_O \quad (3)$$

The voltage stress of D_e and D_f are given below.

$$V_{D_e} = \max(V_1, V_2, V_3) \quad (4)$$

$$V_{D_f} = \frac{V_o}{2} \quad (5)$$

The voltage stress of D_a, D_b, and D_c is given below.

$$V_{Da} = V_{D_b} = \frac{V_O}{4} \quad (6)$$

$$V_{D_c} = \max(V_1, V_2, V_3) \quad (7)$$

Current stress refers to the highest current that flows through a power electronic switch. This current is at its peak when the load is supplied from only one source and the other two power sources are turned off.

The current stress of S_1, S_2, S_3, and S_4 are below.

$$I_{S_1} = I_{S_2} = I_{S_3} = I_{S_4} = 2I_{L_P} = 2(I_{L_{avg}} + \frac{\Delta I_L}{2}) \quad (8)$$

(I_{L_P} Denotes the highest peak value of the inductor current)

The peak current of the inductances L_1 and L_2 is equivalent to the stress current of diodes (D_a, D_b, D_c, D_1, and D_2.

$$I_{D_a} = I_{D_b} = I_{D_c} = I_{D_1} = I_{D_2} = I_{L_P} = I_{L_{avg}} + \frac{\Delta I_L}{2} = I_{L_{avg}} + \frac{(I_{L\max} - I_{L\min})}{2} \quad (9)$$

3 Control Structure

The closed-loop operation with a double-loop PI controller is shown in Fig 4. The outer Loop and inner loop make up the control system. The inductor current (i_L) and output voltage (V_O) are used to determine the control variable β, which denotes the duration of the ON time, that will be applied to S_4. The percentage of power that is transmitted from each source to the load can be represented by the factor (K_i), which represents the ratio between the individual powers (P_{o1}, P_{o2}, P_{o3}) to the total power (P_T).

$$k_1 = \frac{P_{o1}}{P_T} \quad (10)$$

$$k_2 = \frac{P_{o2}}{P_T} \quad (11)$$

$$k_3 = \frac{P_{o1}}{P_T} \quad (12)$$

$$k_T = k_1 + k_2 + k_3 = 1 \quad (13)$$

According to the comparison between the control signal (V_C) that is produced from the second-loop PI controller and the bipolar sawtooth signal with an amplitude of one the duty cycle (D_4) applied for (S_4)can be obtained, as shown in equations (15):

$$\begin{Bmatrix} V_C = 2D_4 - 1 \\ D_4 = \frac{V_C+1}{2} \end{Bmatrix} \quad (14)$$

similarly, the duty cycle (D_1) applied for (S_1) can be obtained by the comparison of the control signal (V_{C1}) and the bipolar sawtooth signal with an amplitude of one, when (D_1)is assumed to be the (K_1 D_4), it can be represented by the equations (16):

$$\begin{Bmatrix} V_{C1} = 2D_1 - 1 \\ D_1 = K_1 D_4 \\ V_{C1} = K_1(V_C + 1) - 1 \end{Bmatrix} \quad (15)$$

Also, the duty cycle (D_2`) can be obtained by comparison of the control signal ($V_{C2}$) and the bipolar sawtooth signal with an amplitude of one, when ($D_2$`)is assumed to be the (($K_1 + K_2$)D_4), it can be represented by the equations (17):

$$\left\{\begin{array}{c} V_{C2} = 2D_2` - 1 \\ D_2` = (K_1 + K_2)D_4 \\ V_{C2} = (K_1 + K_2)(V_C + 1) - 1 \end{array}\right\} \quad (16)$$

The Exclusive OR gate is used between the resulting duty cycles ($D_1$and D_2`) and the output with duty cycle $D_2$ is applied for $S_2$, and also another is used between ($D_2$`and D_4) and the output is applied with duty cycle $D_3$for S_3, in order to avoid the overlapping between the input sources and ensure sequential operation.

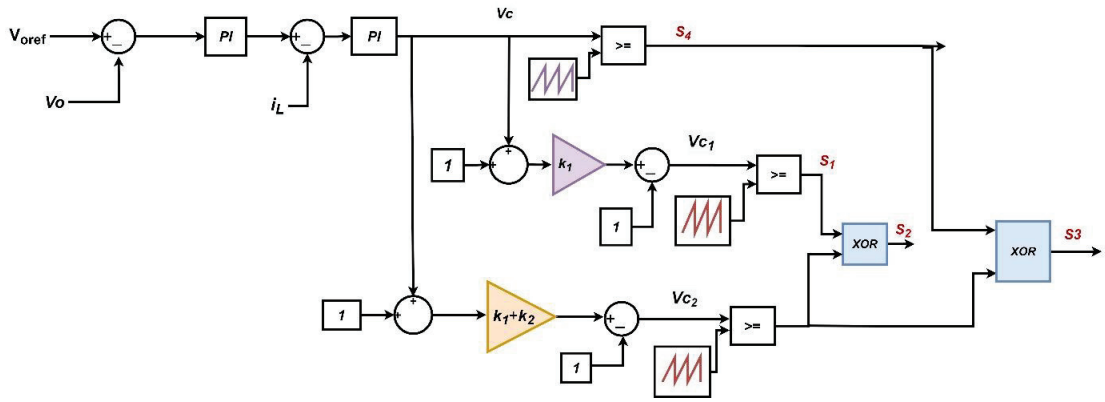

Fig. 4. The operational control structure of the converter

The closed-loop transfer function of the block diagram of the control system shown in Fig. 5 is derived as follows:

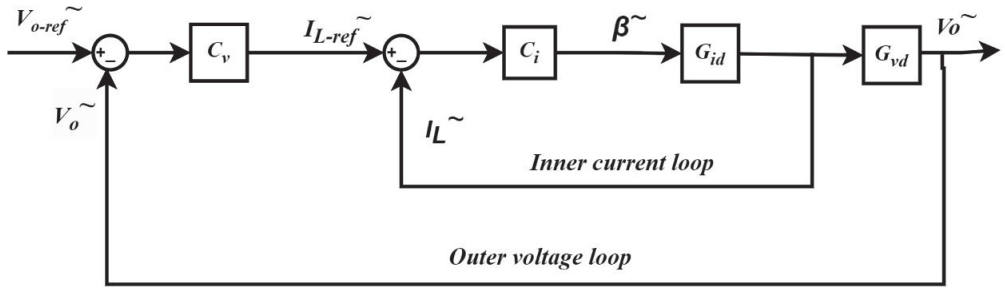

Fig 5. The block diagram of the closed-loop control system

$$\frac{di_L}{dt} = \frac{V_1}{L} \quad at\ D_1 \quad (17)$$

$$\frac{di_L}{dt} = \frac{V_2}{L} \quad at\ D_2 \quad (18)$$

$$\frac{di_L}{dt} = \frac{V_3}{L} \quad at\ D_3 \quad (19)$$

$$\frac{di_L}{dt} = \frac{-vo}{4L} \quad \text{at } (1 - \sum_{i=1}^{3} D_i) \quad (20)$$

$$\frac{di_L}{dt} = \frac{\sum_{i=1}^{3} V_i D_i - \frac{vo}{4}\ (1 - \sum_{i=1}^{3} D_i)}{L} \quad (21)$$

$$\beta = \sum_{i=1}^{3} D_i \quad (22)$$

$$\gamma = \sum_{i=1}^{3} V_i \; D_i \quad (23)$$

$$\begin{Bmatrix} \frac{di_L}{dt} = \frac{\gamma + \frac{vo}{4}\beta}{L} - \frac{Vo}{4L} \\ \frac{dV_o}{dt} = \frac{i_L(1-\beta)}{C} - \frac{V_o}{RC} \end{Bmatrix} \quad (24)$$

According to the small signal modeling approach, the inductor current (i_L), output voltage (Vo), duty cycles, and input voltages can be divided into two components: DC values (I_L, V_o, β, and γ) and disturbance values ($i_L{}^{\sim}$, $v_o{}^{\sim}$, $\beta^{\sim}$,$\gamma^{\sim}$).

$$i_L(t) = I_L + i_L{}^{\sim}(t) \quad (25)$$

$$v_o(t) = V_O + v_o{}^{\sim}(t) \quad (26)$$

$$\beta(t) = \beta + \beta^{\sim}(t) \quad (27)$$

$$\gamma(t) = \gamma + \gamma^{\sim}(t) \quad 28$$

Then substitute eq (26,27,28 and 29) in equations (25) and neglecting the multiplied disturbance terms gives:

$$\frac{d\, i_L{}^{\sim}(t)}{dt} = \frac{V_o\ \beta^{\sim}(t)}{4L} - \frac{v_o{}^{\sim}(t)(1-\beta)}{4L} + \frac{\gamma^{\sim}(t)}{L} \quad (29)$$

$$\frac{dv_o{}^{\sim}(t)}{dt} = \frac{i_L{}^{\sim}(t)(1-\beta) - I_L\,\beta^{\sim}(t)}{C} - \frac{v_o{}^{\sim}(t)}{RC} \quad (30)$$

Take Laplace Transform for equation (28) and (29)

$$i_L{}^{\sim}(s) = \frac{V_o\,\beta^{\sim}(s)}{4Ls} - \frac{v_o{}^{\sim}(s)(1-\beta)}{4Ls} + \frac{\gamma^{\sim}(s)}{Ls} \quad (31)$$

$$v_o{}^{\sim}(s) = \frac{i_L^{\sim}(s)(1-\beta) - I_L\,\beta^{\sim}(s)}{C\left(s + \frac{1}{RC}\right)} \quad (32)$$

$$V_o = \frac{4\gamma}{(1-\beta)} \quad (33)$$

$$I_L = \frac{16\gamma}{(1-\beta)^2 R} \quad (34)$$

Substitute eq (33), (34), and (35) in eq (32)

$$i_L{}^{\sim}(s) = \frac{\gamma^{\sim}(s)}{Ls} + \frac{\gamma\ \beta^{\sim}(s)}{Ls(1-\beta)} - \frac{i_L{}^{\sim}(s)(1-\beta)^2}{4LsC\left(s + \frac{1}{RC}\right)} + \frac{4\gamma}{LCRS\left(s + \frac{1}{RC}\right)(1-\beta)} \quad (35)$$

The transfer function $G_{id}(s)$ representing the relationship between the inductor current and the duty cycle ''$i_L{}^{\sim}(s)\backslash\ \beta^{\sim}(s)$'' can be derived using equation (37)

$$G_{id}(s) = \frac{i_L{}^{\sim}(s)}{\beta^{\sim}(s)}\Big|_{\gamma^{\sim}=0} = \frac{\frac{\gamma}{Ls(1-\beta)} + \frac{4\gamma}{LCRS(1-\beta)\left(s+\frac{1}{RC}\right)}}{1 + \frac{(1-\beta)^2}{4LCs\left(s+\frac{1}{RC}\right)}} \quad (36)$$

Similarly, transfer function between output voltage and the inductor current''$vo^{\sim}(s)\backslash i_L{}^{\sim}(s)$'' is obtained as follows :

$$G_{Vd}(s) = \frac{vo^{\sim}(s)}{i_L{}^{\sim}(s)}\Big|_{\beta^{\sim}=0} = \frac{(1-\beta)}{C\left(s+\frac{1}{RC}\right)} \quad (37)$$

$$C_V(s) = K_{Pv} + \frac{K_{iv}}{S} \quad (38)$$

(K_{Pv} Voltage proportional gain, K_{iv}: Voltage integral gain)

$$C_i(s) = K_{Pi} + \frac{K_{ii}}{S} \quad (39)$$

(K_{Pi}: current proportional gain, K_{ii}: Voltage integral gain)

$$\frac{V_o{}^{\sim}}{V_{oref}{}^{\sim}} = \frac{C_v(s)\ C_i(s) G_{id}(s) G_{Vd}(s)}{1 + C_i(s) G_{id}(s) + C_v(s)\ C_i(s) G_{id}(s) G_{Vd}(s)} \quad (40)$$

3.1 DC Voltage Balancing Control

Fig.6. show the voltage balancing control that is necessary for bipolar symmetric output DC-to-DC converters to maintain output symmetry under changing load conditions or input voltage. The positive and negative output voltages are compared and the difference is applied to the proportional-integral (PI) controller to produce a signal which is compared with the sawtooth signal to produce control pulses for the switch S_p and inverted signal ($S_n = \overline{S_p}$) for the switch S_n. The switching frequency is 50 kHz and the gains of the proportional integral controller are 0.0001 for proportional gain and 0.3 for integral gain.

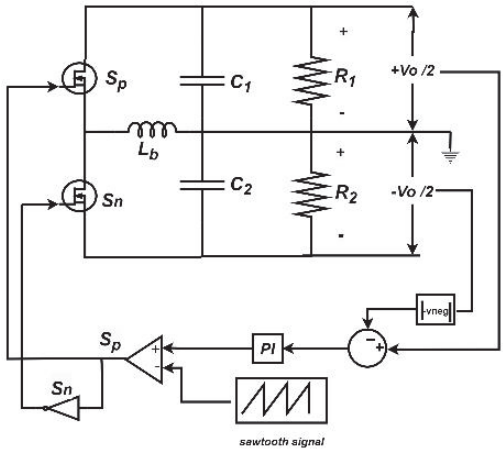

Fig.6. Control circuit for voltage balancing.

4 4. Simulation Results and Discussions

The topological structure of the proposed converter was analyzed during closed-loop operation to ensure that the output voltage remained constant at $\pm V_o/2$ and V_o with ±200 V and 400 V, respectively. When the load and duty cycles for switches are different, even when there are a lot of changes, the controller is capable of maintaining the output voltage in close proximity to the reference value. Closed-loop operations were evaluated throughout four scenarios. In the first scenario, power is sent at the same time from three sources with both the same and different voltage levels. This shows how the suggested converter would work. In the end, it was seen that power was flowing from all three sources (V_1, V_2, and V_3) to the dc link independently. The duty cycles provided for S_1, S_2, and S_3 in four different scenarios can be expressed as a percentage of the total duty cycle D_4 generated by the closed-loop control system that is used for S_4. They are as suggested, D_1 = 60%, D_2 = 20%, and D_3 = 20% of D_4 according to the percentage of power that is transmitted from each source to the load which was calculated from the factor (K_i) using Equations (11,12,13). Table 1 displays the parameters that were used in the proposed converter.

Table 1. Parameters Used in The Proposed Converter

Parameter	Values
Switching Frequency F_s	50 kHz
Input Voltage1	150 V
Input Voltage2	100 V
Input Voltage3	75 V
Output voltages $\pm V_o/2$, V_o	±200V,400V
Total Resistance R_t	320 Ω
Resistors $R_1 = R_2$	160 Ω
Inductors $L_1 = L_2 = L_b$	1mH

Capacitors C_1 =C_2	10 μF
Voltage proportional gain K_{Pv}	0.06
Voltage integral gainK_{iv}	80
Current proportional gain K_{Pi}	0.08
Current integral gain K_{ii}	100

The results of the simulation for the first scenario are shown in Fig. 7. Due to a difference in input voltages, (V_1 = 150 V, V_2 = 100 V, and V_3 = 75 V), the voltage sources will operate in a sequential manner, starting from the V_1 and decreasing to the V_3, in accordance with their respective duty cycles. voltage balance control supplies the duty cycles to the bipolar dc bus switches S_p and S_n. For the purpose of verification, a resistive load of 160Ω was applied to a two-level bipolar dc bus, and 320Ω for the total load. The output voltages and currents for two bipolar dc bus $\pm Vo/2$ are about $\pm 200V$ while the current is $\pm$1.25 A respectively. The total output voltage and total output current are about (V_O =400V, and I_O=1.25A) respectively. Equal currents and voltages flow through L_1 and L_2 ($I_{L_1} = I_{L_2}, V_{L_1} = V_{L_2}$), the voltages flow through L_b during the first part of the period is $V_o/2$ with 200V and -$V_o/2$ with -200V during the second part of the period, the average current and the peak-to-peak ripple current for L_1, L_2, and L_b, respectively :($I_{L_1} = I_{L_2} = 9.45A, I_{L_b} = 5A, \Delta i_{L1} = \Delta i_{L2} = 1.1\ A, \Delta i_{Lb} = 2\ A$), and the peak to peak ripple voltages at steady state for $\pm Vo/2$ and V_O, respectively (Δv_{o1} =6.5V, Δv_{o2} =2.5V, and Δv_o =9V). During the operation of S_1, the voltage of S_2 has a negative value, about – 50 V, which is V_2–V_1, due to the blocking action of its reverse current, S_3 has a negative voltage, about – 75 V, which is V_3–V_1, because of its reverse current-blocking. Moreover, during the operation of S_2, the voltage across S_1 is around 50 V, resulting from the difference between V_1 and V_2, due to the reversal of its blocking action. Similarly, the voltage across S_3 is negative, approximately -25V, resulting from the difference between V_3 and V_2, due to its reverse current blocking property. During the operation of S_3, the voltage across S_1 is around 75 V, resulting from the difference between V_1 and V_3, attributable to its reverse blocking characteristics. Similarly, the voltage across S_2 is approximately 25 V, arising from the difference between V_2 and V_3, owing to its reverse current blocking properties, the voltage across S_4 during the second part of the period is $V_o/2$ with 200V.The current and voltage for switches (i_{S1}, i_{S2}, i_{S3}, V_{S1}, V_{S2}, and V_{S3}) are depicted in Figure 7.

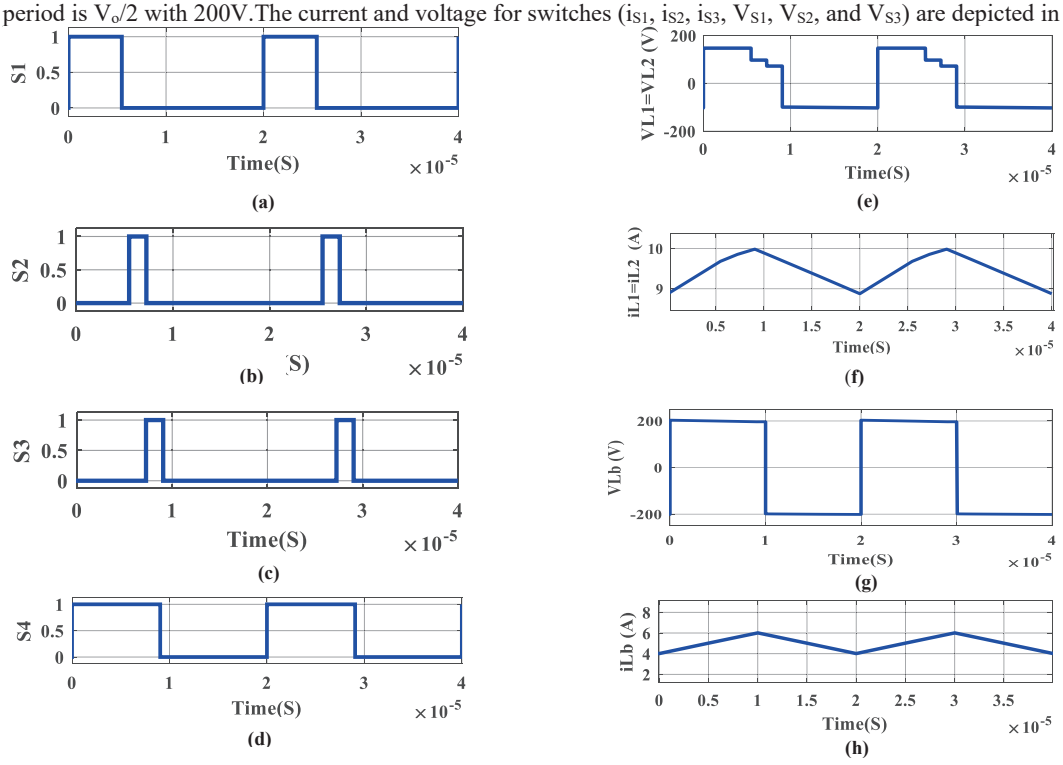

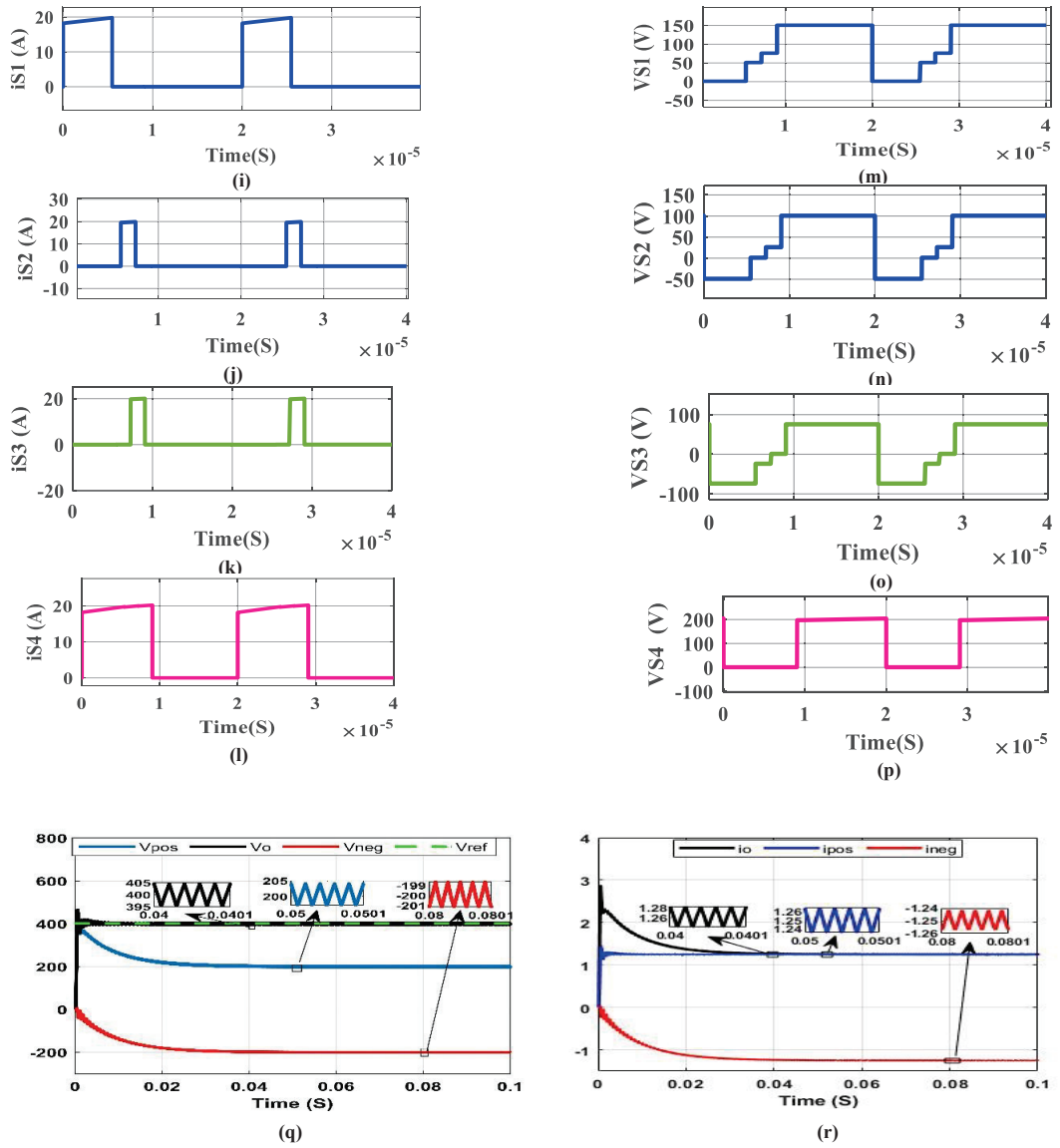

Fig. 7.
The simulation results when three sources (V_1=150V, V_2=100V, V_3=75): the waveform of switches control pulses (a)S_1, (b)S_2, (c)S_3, and (d) S_4; the voltages and currents across L_1, L_2, and L_b (e) V_{L1} and V_{L2}, (f) i_{L1} and i_{L2} (g) V_{Lb}, and (h) i_{Lb}; the voltages and currents across switches (S_1, S_2, S_3, S_4) (i) i_{S1}, (j)i_{S2}, (K) i_{S3}, and (l) i_{S4} (m)V_{S1}, (n) V_{S2}, (o) V_{S3}, and (p)V_{S4}; (q)output voltages, and (r)output currents.

In Fig.8, the scenario involves the simultaneous transmission of power from three sources to the load. Equal input voltages are provided, denoted as $V_1 = V_2 = V_3 = 100$V. In the case of equal sources, a sequential operation is noticed due to the action of the Exclusive OR gate in closed-loop control to prevent the operation of multiple sources at the same time. Consequently. The simulation results indicate that the output voltages, for $\pm V_o/2$ and V_o are $\pm 200V$ and 400V, respectively. Additionally, the corresponding currents are$\pm$1.25A. L_1 and L_2 both have the same magnitude of current and voltage. ($I_{L_1} = I_{L_2}, V_{L_1} = V_{L_2}$), the average current and the peak-to-peak current for L_1, L_2, and L_b, respectively: ($I_{L_1} = I_{L_2} = 10.5, I_{L_b} = 5A, \Delta i_{L1} = \Delta i_{L2} = 1\ A, \Delta i_{Lb} = 2\ A$) and the peak to peak ripple voltages at steady state for $\pm$Vo/2 and V_O, respectively ($\Delta v_{o1} = 8$V, $\Delta v_{o2} = 2.5$V, and $\Delta v_o = 10$V).

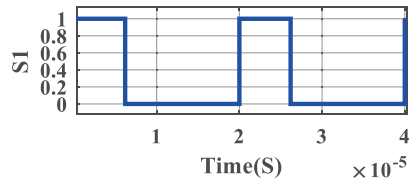

(a)

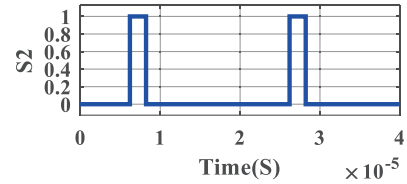

(b)

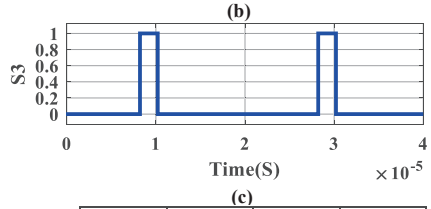

(c)

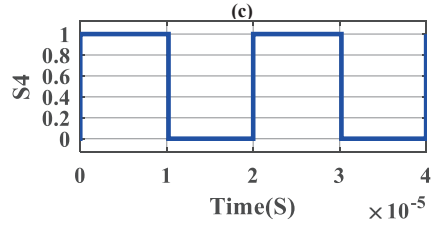

(d)

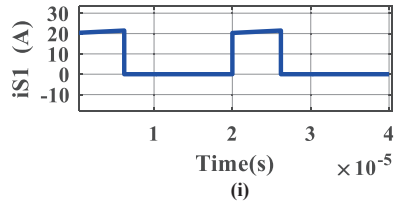

(i)

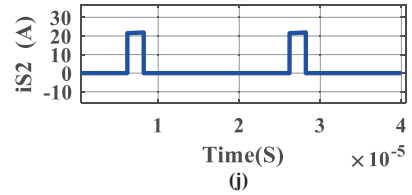

(j)

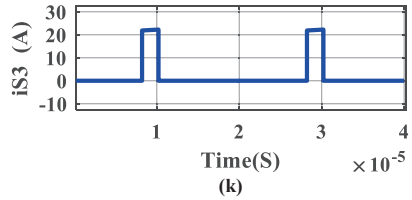

(k)

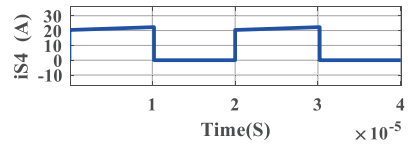

(l)

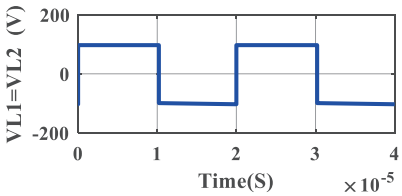

(e)

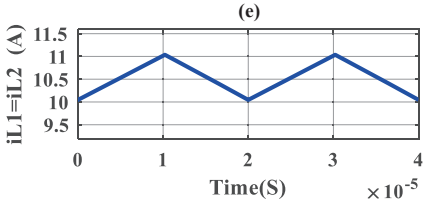

(f)

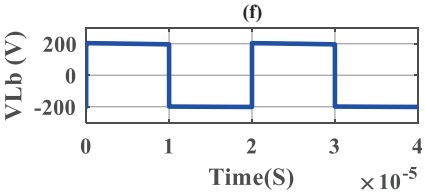

(g)

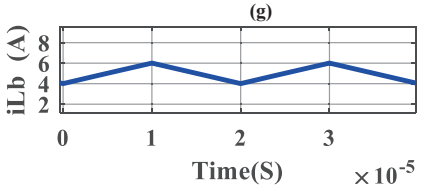

(h)

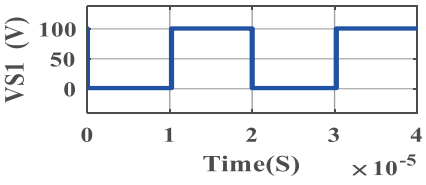

(m)

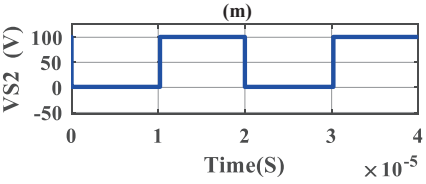

(n)

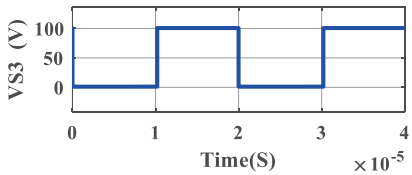

(o)

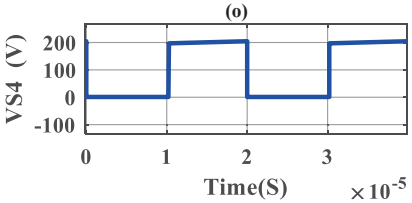

(p)

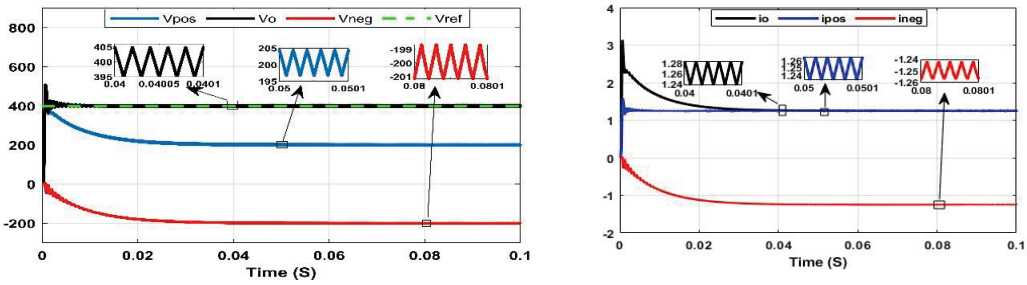

Fig. 8. The simulation results when equal three sources V_1= V_2= V_3 =100V: the waveform of switches control pulses (a)S_1, (b)S_2, (c)S_3, and (d) S_4; the voltages and currents across L_1, L_2, and L_b (e) V_{L1} and V_{L2}, (f) i_{L1} and i_{L2} (g) V_{Lb}, and (h) i_{Lb}; the voltages and currents across switches (S_1, S_2, S_3, S_4) (i) i_{S1}, (j)i_{S2}, (K) i_{S3}, and (l) i_{S4} (m)V_{S1}, (n) V_{S2},(o) V_{S3}, and (p)V_{S4} ; (q)output voltages, and (r)output currents.

As shown in Fig. 9. Power is transferred to the load from only two inputs in this scenario. In the event of an unavailability of one of these sources, energy will be transferred from the remaining two sources. Balanced output voltages are maintained even in the presence of just two inputs. The simulation results indicate that the output voltages for $\pm V_O/2$ and V_O are $\pm 200V$ and 400V, respectively. Additionally, the corresponding currents are$\pm$1.25A. L_1 and L_2 both have the same magnitude of current and voltage. ($I_{L_1} = I_{L_2}, V_{L_1} = V_{L_2}$) , the average currents and the peak-to-peak ripple currents for L_1, L_2, and L_b, respectively:($I_{L_1} = I_{L_2} = 9.25A, I_{L_b} = 5A, \Delta i_{L1} = \Delta i_{L2} = 1.1\ A, \Delta i_{Lb} = 2\ A$) and the peak to peak ripple voltages at steady state for $\pm$Vo/2 and V_O, respectively ($\Delta v_{o1} = 7\text{V}$, $\Delta v_{o2} = 2.5\text{V}$ and $\Delta v_o = 8\text{V}$).

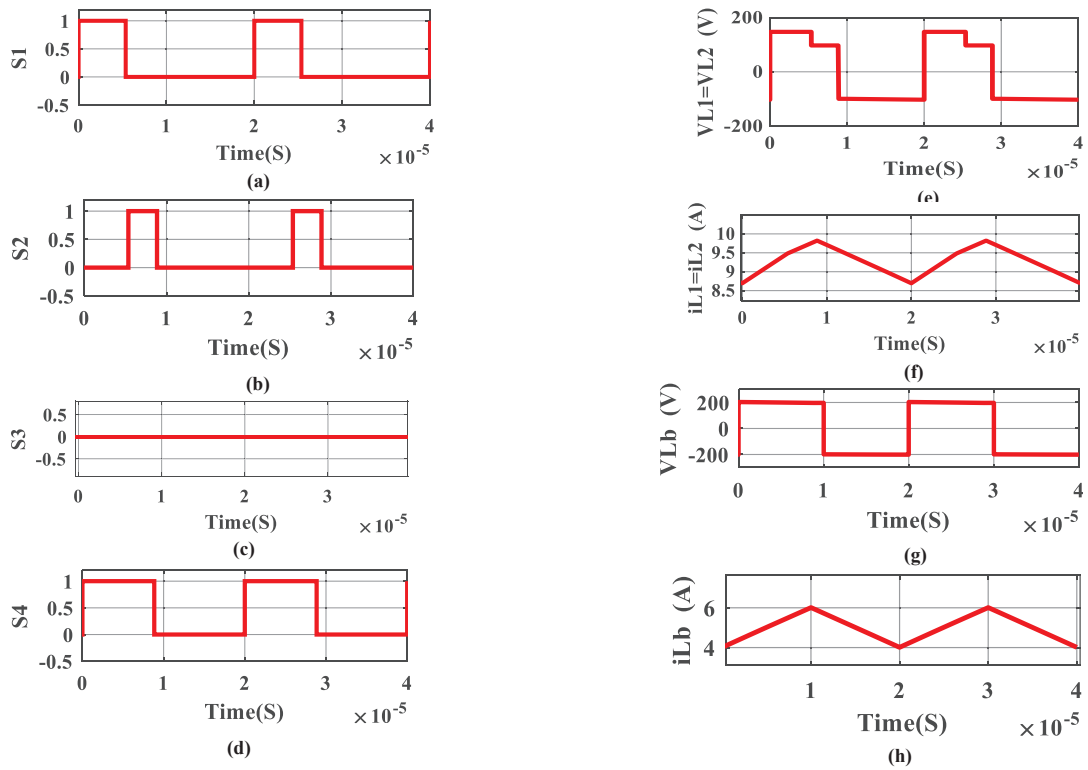

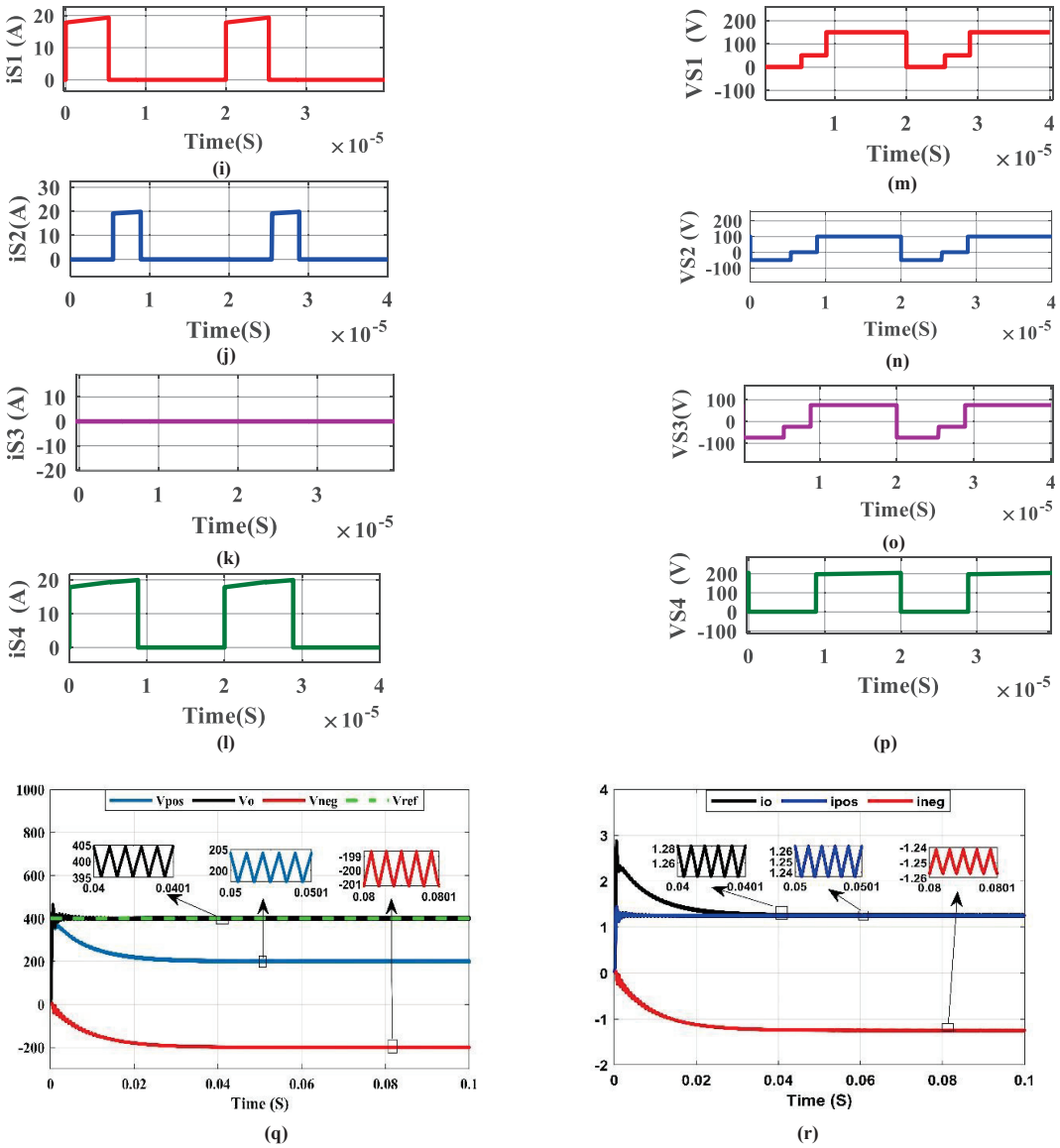

Fig. 9. The simulation results when only two sources (V_1= 150V and V_2= 100V) are used: the waveform of switches control pulses (a)S_1, (b)S_2, (c)S_3, and (d) S_4; the voltages and currents across L_1, L_2, and L_b (e) V_{L1} and V_{L2}, (f) i_{L1} and i_{L2} (g) V_{Lb}, and (h) i_{Lb}; the voltages and currents across switches (S_1, S_2, S_3, S_4) (i) i_{S1}, (j)i_{S2}, (K) i_{S3}, and (l) i_{S4} (m)V_{S1}, (n) V_{S2}, (o) V_{S3}, and (p)V_{S4} ; (q)output voltages, and (r)output currents.

In Fig.10. Within this scenario, power flows independently from the input sources. With V_1=150V, only V_1 supplies to the load. If only one source is available, both output voltages don't change; they stay balanced. In the simulation, the output voltages $\pm V_o/2$ and V_o are $\pm 200V$ and 400V, respectively. Additionally, the corresponding currents are$\pm$1.25A. L_1 and L_2 both have the same magnitude of current and voltage ($I_{L_1} = I_{L_2}, V_{L_1} = V_{L_2}$), the average current and the peak-to-peak ripple current for L_1, L_2, and L_b, respectively: ($I_{L_1} = I_{L_2} = 8.5A, I_{Lb} = 5A, \Delta i_{L1} = \Delta i_{L2} = 0.4\ A,\ \Delta i_{Lb} = 2\ A$)and the peak to peak ripple voltages at steady state for $\pm$Vo/2 and V_O, respectively ($\Delta v_{o1} = 17\text{V},\ \Delta v_{o2} = 5.5\text{V}$ and $\Delta v_o = 20\text{V}$).

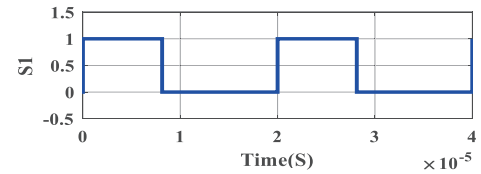

(a)

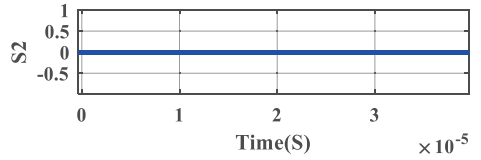

(b)

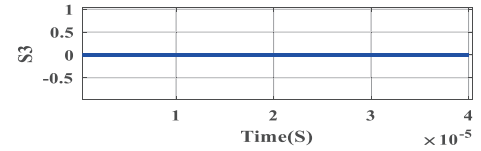

(c)

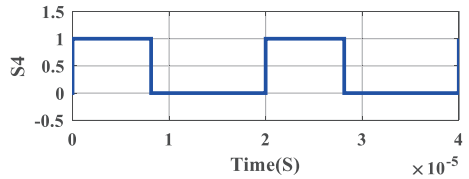

(d)

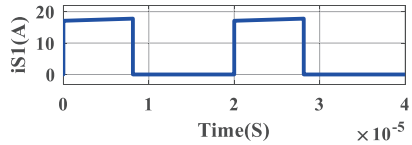

(i)

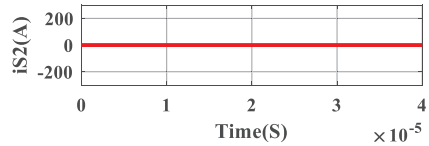

(j)

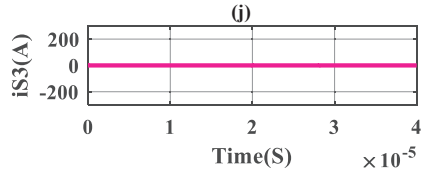

(k)

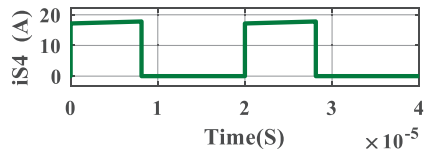

(l)

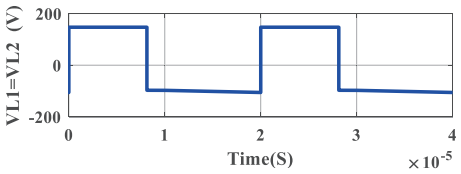

(e)

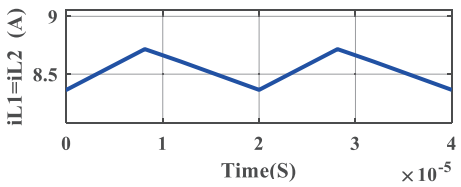

(f)

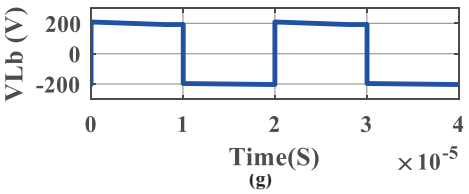

(g)

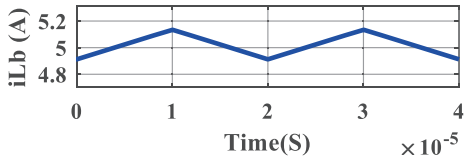

(h)

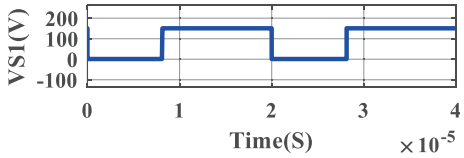

(m)

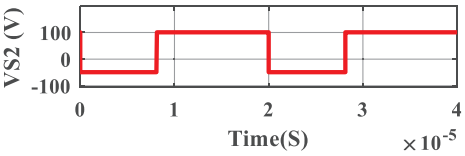

(n)

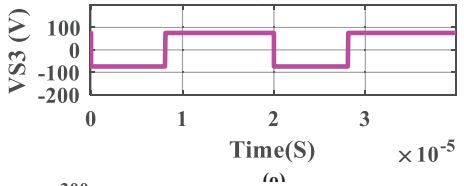

(o)

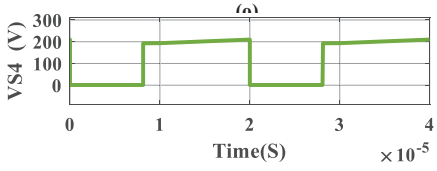

(p)

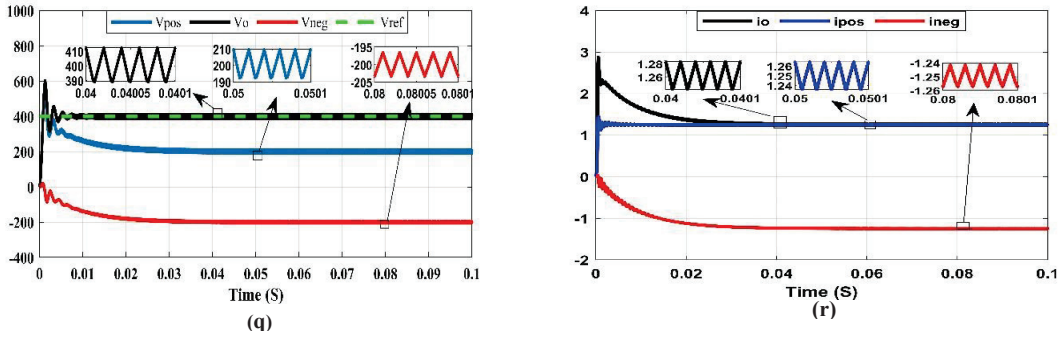

Fig. 10. The simulation results when only (V_1=150V) is used: the waveform of switches control pulses (a)S_1, (b)S_2, (c)S_3, and (d) S_4; the voltages and currents across L_1, L_2, and L_b (e) V_{L1} and V_{L2}, (f) i_{L1} and i_{L2} (g) V_{LB}, and (h) $i_{LB;\ the}$ voltages and currents across switches (S_1, S_2, S_3, S_4) (i) i_{S1}, (j)i_{S2}, (K) i_{S3}, and (l) i_{S4} (m)V_{S1},(n) V_{S2},(o) V_{S3}, and (p)V_{S4} ; (q)output voltages, and (r)output currents.

4.1 Verification of Operation with Unbalanced Load

The proposed converter was tested with varied positive and negative pole loads. Fig. 11 contains a presentation of the results of the simulation at unbalanced loads when (R_1=200 Ω, and R_2=400 Ω) with V_1 = 150 V, V_2 = 100 V, and V_3 = 75 V. It was shown from the results, that even if the load increases in one of the poles, the output voltages ($\pm V_O/2$) will be balanced at a value of (±200) and do not change. The output currents are about (I_{pos} =+1A, and I_{neg} = - 0.5A), the peak-to-peak ripple voltages at steady state for V_O and $\pm$ Vo/2, respectively ($\Delta v_o = 6$V, $\Delta v_{o1} = 4$V, and $\Delta v_{o2} = 1.6$V). The primary benefit of the proposed converter even if the loads are unbalanced, the output voltages are the same.

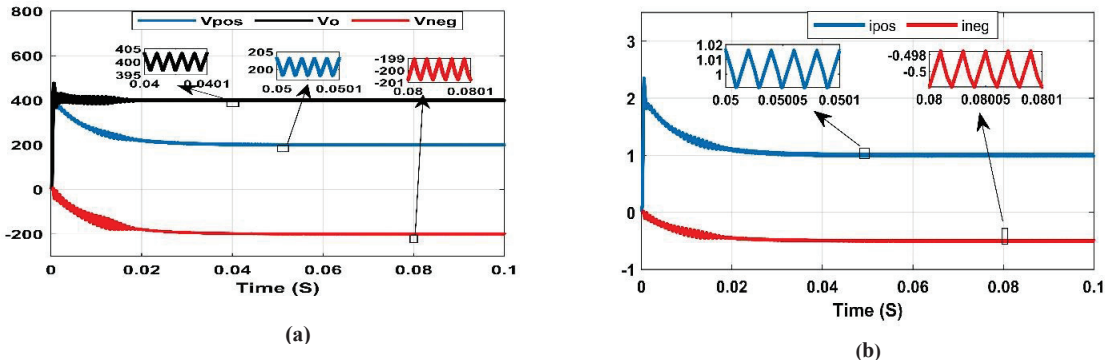

Fig.11. The simulation results of output voltages and output currents with three voltage sources (V_1=150V, V_2=100V, V_3=75) supply to the load at unbalanced (R_1 = 200 Ω, R_2 = 400 Ω) (a) V_{pos}, V_{neg}, Vo (b) i_{pos}, i_{neg}.

Fig. 12 shows simulation results for a sudden change in the total load R_t, that was made from 320 Ω to 640 Ω at t = 0.035 s, while the power output decreased from 500 W to 250 W, then from 640Ω to 320Ω at t = 0.07 s, resulting in an increase in power from 250 W to 500W. Because of a sudden change in the load at t = 0.035 s and t = 0.07 s, output voltages and currents (V_{pos}, V_{neg}, V_o, i_{pos}, i_{neg}) show slight overshoot and downshoot but immediately settles to desired values and the controller reacts instantly, adjusting the duty cycles to provide an output voltage of 400 V. The resistors across the positive and negative poles do not change (R_1=R_2=160 Ω). The results show that when the power at the total load decreases from rated 500W to half the value, and also when it increases from half the value to rated, the output voltages ($\pm V_O/2$) are not affected and remain balanced at values of (±200) in both cases, and the peak to peak ripple voltages at steady state for $\pm$Vo/2 and V_O, respectively ($\Delta v_{o1} = 4$V, $\Delta v_{o2} = 1.6$V, and $\Delta v_o = 6$V) and the currents (i_{pos}= i_{neg}= ±1.25A). Table 2 displays the three different work conditions.

Table 2. Various Working Conditions

Time	Total load	Total power	Total current

0 – 0.035 s	320 Ω	500W	1.25A
0.035 – 0.07 s	640 Ω	250W	0.625A
0.07 -0.1 s	320 Ω	500W	1.25A

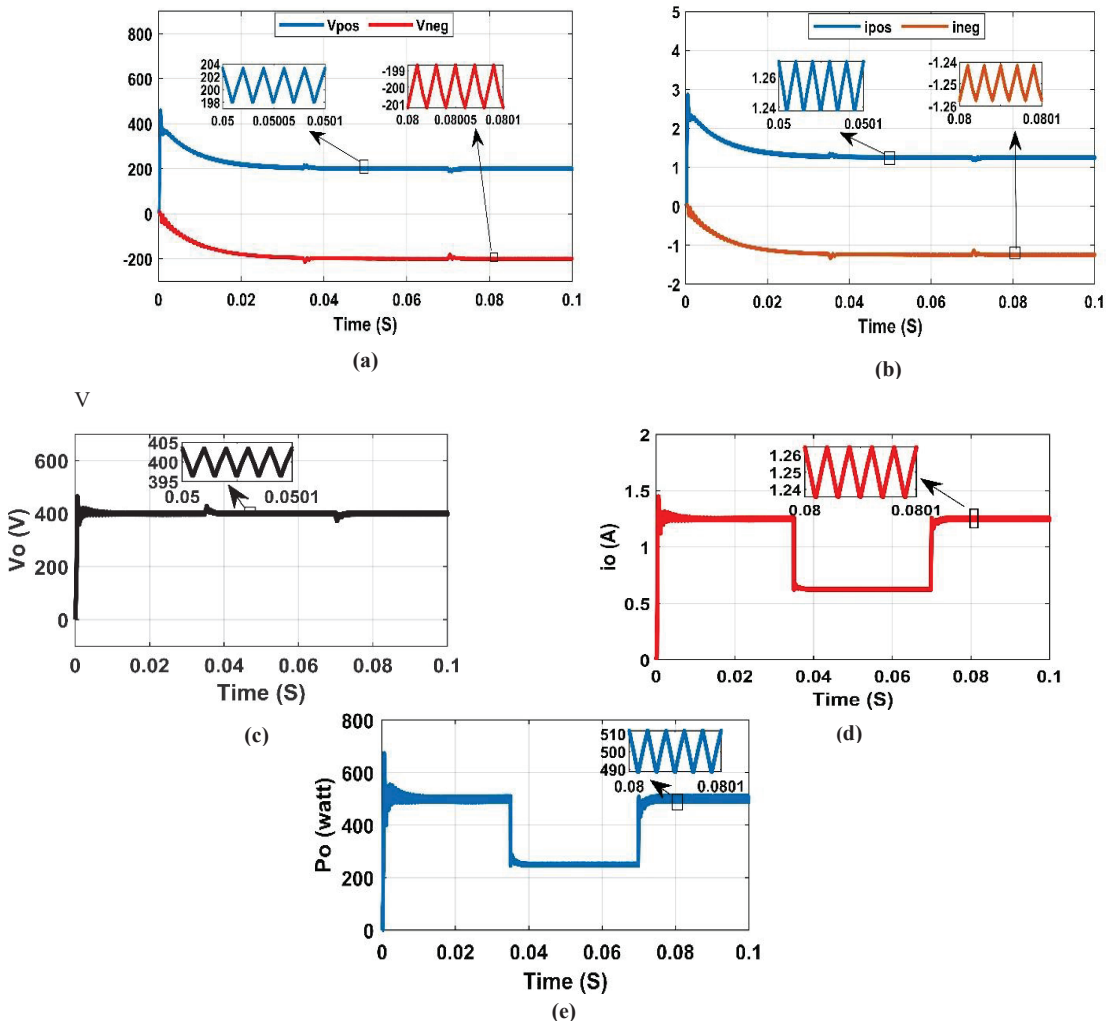

Fig .12. The simulation results for changing load with three voltage sources (V_1=150V, V_2=100V, V_3=75) (a) The output voltages V_{pos}, V_{neg}, (b) The output currents i_{pos}, i_{neg}, (c)The output voltage V_O, (d) The output current i_O, and (e) The output power P_O.

5 Conclusion

This study introduces a proposed non-isolated DC to DC converter with three inputs and bipolar symmetric outputs. The performance of the suggested converter has been evaluated in a closed-loop configuration to maintain a constant output voltage of ±Vo/2. The values of ±Vo/2 and Vo considered in the analysis are ±200 V and 400 V, respectively. The suggested converter works with power transfer independently or simultaneously from three sources, each supplying an equal and unequal voltage level to the dc link. The Exclusive OR gates are used to connect the supply voltage sources in a sequential manner whether the inputs are the same or different voltages and prevent the overlap operation of three sources. Voltages were connected one after another, from the first to the last voltages, with each source operating according to the duty cycle provided for it. A voltage balancer is used in the converter to maintain a stable and balanced operation of the system, even when the load and duty cycles for switches change suddenly. In order to test and confirm

the results of the proposed converter, a MATLAB/Simulink program is used. According to the results of simulations, this converter provides the following set of advantages: It is possible to achieve high voltage gain, and power of (1000W), regardless of whether the power is coming from three sources, two sources, or just one source.

References

1. Ravada, Bhaskara Rao, Narsa Reddy Tummuru, and Bala Naga Lingaiah Ande. " PV-Wind and Hybrid Energy Storage Integrated Multi-Source Converter Configuration based Grid-interactive Microgrid." *IEEE Transactions on Sustainable Energy*, vol. 12, no. 1, pp. 83-91, (2020), doi:10.1109/tie.2020.2984437.
2. Rafiei, Mehdi, Jalil Boudjadar, and Mohammad-Hassan Khooban. " Energy Management of a Zero-Emission Ferry Boat with a Fuel Cell-Based Hybrid Energy System: Feasibility Assessment." *IEEE Transactions on Industrial Electronics*, vol.68, no. 2, pp. 1739-1748, (2020), doi:10.1109/tie.2020.2992005.
3. Almutairi, Abdulaziz, Khairy Sayed, Naif Albagami, Ahmed G. Abo-Khalil, and Hedra Saleeb. " Multi-Port PWM DC-DC Power Converter for Renewable Energy Applications." *Energies*, vol.14, no. 12, p.3490, (2021), doi:10.3390/en14123490.
4. Jiya, Immanuel N., Ahmed Salem, Huynh Van Khang, Nand Kishor, and Rade Ciric. " Novel multisource DC-DC converter for All-electric hybrid energy systems." *IEEE Transactions on Industrial Electronics*, vol.69, no. 12, pp.12934-12945, (2021), doi:10.1109/TIE.2021.3131871.
5. Chen, Guipeng, Zhufeng Jin, Yuwei Liu, Yihua Hu, Jiangfeng Zhang, and Xinlin Qing. " Programmable Topology Derivation of Integrated Three-Port DC-DC Converters with Reduced Switches for Low-Cost Applications." *IEEE Transactions on Industrial Electronics*, vol. 66, no. 9, pp.6649-6660, (2018), doi:10.1109/TIE.2018.2877159.
6. Faraji, Rasoul, and Hosein Farzanehfard. " Soft-switched Non-Isolated High Step-up Three-port DC-DC Converter for Hybrid Energy Systems." *IEEE Transactions on Power Electronics*, vol.33, no. 12, pp.10101-10111, (2018), doi:10.1109/tpel.2018.2791840.
7. Saadatizadeh, Zahra, Pedram Chavoshipour Heris, and H. Alan Mantooth. " Modular Expandable Multiinput Multioutput (MIMO) High Step-Up Transformerless DC-DC Converter." *IEEE Access*, vol.10, pp. 53124-53142, (2022), doi: 10.1109/ACCESS.2022.3175876.
8. Zhang, Hao, Dachu Dong, Min Jing, Wei Liu, and Feng Zheng. " Topology Derivation of Multiple-Port DC-DC Converters Based on Voltage-Type Ports." *IEEE Transactions on Industrial Electronics*, vol.69, no. 5, pp.4742-4753, (2021), doi:10.1109/tie.2021.3078389.
9. Alajmi, Bader N., Mostafa I. Marei, Ibrahim Abdelsalam, and Mohamed F. AlHajri. " Analysis and Design of a Multi-Port DC-DC Converter for Interfacing PV Systems." *Energies*, vol.14, no. 7, p. 1943, (2021), doi:10.3390/en14071943.
10. Li, Xiaolu Lucia, Zheng Dong, K. Tse Chi, and Dylan Dah-Chuan Lu. " Single-Inductor Multi-Input Multi-Output DC-DC Converter with High Flexibility and Simple Control." *IEEE Transactions on Power Electronics*, vol.35, no. 12, pp.13104-13114, (2020), doi:10.1109/tpel.2020.299135.
11. Lavanya, A., R. Jegatheesan, and K. Vijayakumar. " Design of Novel Dual Input DC–DC Converter for Energy Harvesting System in IoT Sensor Nodes." *Wireless Personal Communications*, vol.117, no. 4, pp.2793-2808, (2021), doi:10.1007/s11277-020-07048-0.
12. Bharathidasan, Mohan, Vairavasundaram Indragandhi, and Belqasem Aljafari. " Hybrid Controlled Multi-Input DC/DC Converter for Electric Vehicle Application." *International Transactions on Electrical Energy Systems*, *2023*, doi:10.1155/2023/8308418.
13. Harini, S., N. Chellammal, Bharatiraja Chokkalingam, and Lucian Mihet-Popa. " A novel high gain dual input single output Z-Quasi Resonant (Zqr) Dc/Dc converter for off-board Ev charging." *IEEE Access*, vol.10, pp.83350-83367, (2022), doi:10.1109/ACCESS.2022.3195936.
14. Khan, Muhammad Yasir Ali, Haoming Liu, and Naveed Ur Rehman. " Design of a Multiport Bidirectional DC-DC Converter for Low Power PV Applications." International Conference on Emerging Power Technologies (ICEPT), pp. 1-6. IEEE, 2021, doi:10.1109/icept51706.2021.9435425.
15. Maalandish, Mohammad, Seyed Hossein Hosseini, Mehran Sabahi, Naghi Rostami, and Mohammad-Hassan Khooban. " High step-up multi input–multi output DC–DC converter with high controllability for battery charger/EV applications." *IET Power Electronics*,2023, doi: 10.1049/pel2.12587.
16. Tian, Qingxin, Guohua Zhou, Minrui Leng, Guodong Xu, and Xianyan Fan. " A Nonisolated Symmetric Bipolar Output Four-Port Converter Interfacing PV-Battery System." *IEEE Transactions on Power Electronics*, vol. 35, no. 11, pp.11731-11744, (2020), doi:10.1109/TPEL.2020.2983113.

17. Gu, Yunjie, Wuhua Li, and Xiangning He. " Analysis and Control of Bipolar LVDC Grid with DC Symmetrical Component Method." *IEEE* Transactions on Power Systems, vol.31, no. 1, pp.685-694, (2015), doi:10.1109/tpwrs.2015.2403310.
18. Fernão Pires, Vitor, Armando Cordeiro, Daniel Foito, and José Fernando Silva. " A High-Voltage Gain Non-Isolated DC–DC Converter Designed for Bipolar DC Microgrids " *Electric Power Components and Systems*, vol.51, no. 12, pp.1171-1181, (2023), doi:10.1080/15325008.2023.2196667.
19. Zhou, Xiang, Yue Wang, Laili Wang, Yan-Fei Liu, and Paresh C. Sen. " A Soft-Switching Transformerless DC−DC Converter with Single-Input Bipolar Symmetric Outputs." *IEEE Transactions on Power Electronics*, vol.36, no. 8, pp.8640-8646, (2020), doi:10.1109/tpel.2020.3048230.
20. Rivera, Sebastian, Ricardo Lizana, Samir Kouro, Tomislav Dragičević, and Bin Wu. " Bipolar DC Power Conversion: State-of-the-Art and Emerging Technologies." *IEEE Journal of Emerging and Selected Topics in Power Electronics*, vol.9, no. 2, pp.1192-1204, (2020), doi:10.1109/jestpe.2020.2980994.
21. Dadjo Tavakoli, Saman, Jasem Khajesalehi, Mohsen Hamzeh, and Keyhan Sheshyekani. " Decentralised voltage balancing in bipolar dc microgrids equipped with trans-z-source interlinking converter." *IET Renewable Power Generation*, vol.10, no. 5, pp.703-712, (2016), doi:10.1049/it-rpg.2015.0222.
22. Ferrera, Maria Bella, Salvador P. Litran, Eladio Duran Aranda, and Jose Manuel Andujar Marquez. " A Converter for Bipolar DC Link Based on SEPIC-Cuk Combination." *IEEE Transactions on Power Electronics*, vol.30, no. 12, pp.6483-6487, (2015), doi:10.1109/tpel.2015.2429745.
23. Kakigano, Hiroaki, Yushi Miura, and Toshifumi Ise. " Low-Voltage Bipolar-Type DC Microgrid for Super High-Quality Distribution." *IEEE Transactions on Power Electronics*, vol.25, no. 12, pp.3066-3075, (2010), doi:10.1109/tpel.2010.2077682.
24. Jiya, Immanuel N., Huynh Van Khang, Nand Kishor, and Rade Ciric. " Novel High-Gain Multiport Isolated DC-DC Converter with Bipolar Symmetric Outputs." In *IECON 2022–48th Annual Conference of the IEEE Industrial Electronics Society*, pp. 1-6. IEEE, 2022, doi: 10.1109/IECON49645.2022.9968834.
25. Kolahian, Pouya, Hadi Tarzamni, Amir Nikafrooz, and Mohsen Hamzeh. " A Multi-port DC-DC Converter for Bipolar MVDC Micro-Grid Applications." *IET Power Electronics*, vol.12, no. 7, pp.1841-1849, (2019), doi:10.1049/iet-pel.2018.6031.
26. Litrán, S. P., E. Durán, R. S. Barroso, J. Semião, and M. B. Ferrera. " Analysis of Converters with Bipolar Output for DC Microgrid " IEEE 14th International Conference on Compatibility, Power Electronics and Power Engineering (CPE- POWERING), vol. 1, pp. 13-18, (2020), doi:10.1109/cpe-powereng48600.2020.9161664.
27. Prabhakaran, Prajof, and Vivek Agarwal. " Novel Four-Port DC-DC Converter for Interfacing Solar PV-Fuel Cell Hybrid Sources with Low-Voltage Bipolar DC Microgrids." *IEEE Journal of Emerging and Selected Topics in Power Electronics*, vol.8, no. 2, pp.1330-1340, (2018), doi:10.1109/jestpe.2018.2885613.
28. Chen, Yenan, Ping Wang, Youssef Elasser, and Minjie Chen. " Multicell Reconfigurable Multi-Input Multi-Output Energy Router Architecture." *IEEE Transactions on Power Electronics*, vol.35, no. 12, pp.13210-13224, (2020), doi:10.1109/tpel.2020.2996199.
29. Prabhakaran, Prajof, and Vivek Agarwal. " Novel Boost-SEPIC type Interleaved DC-DC Converter for Mitigation of Voltage Imbalance in a Low Voltage Bipolar DC Microgrid." *IEEE Transactions on Industrial Electronics*, vol.67, no. 8, pp.6494-6504, (2019), doi:10.1109/tie.2019.2939991.
30. Jiya, Immanuel Ninma, Huynh Van Khang, Nand Kishor, and Rade M. Ciric. " Novel Family of High-Gain Nonisolated Multiport Converters with Bipolar Symmetric Outputs for DC Microgrids." *IEEE Transactions on Power Electronics*, vol.37, no. 10,pp.12151-12166, (2022), doi: 10.1109/TPEL.2022.3176688.